Use of Quantitative Mass Spectrometric Analysis to Elucidate the Mechanisms of Phospho-priming and Auto-activation of the Checkpoint Kinase Rad53 *in Vivo**ⓢ

Eric S.-W. Chen‡§¶, Nicolas C. Hoch‖**, Shun-Chang Wang‡, Achille Pellicioli‡‡, Jörg Heierhorst‖**§§, and Ming-Daw Tsai‡§¶§§

The cell cycle checkpoint kinases play central roles in the genome maintenance of eukaryotes. Activation of the yeast checkpoint kinase Rad53 involves Rad9 or Mrc1 adaptor-mediated phospho-priming by Mec1 kinase, followed by auto-activating phosphorylation within its activation loop. However, the mechanisms by which these adaptors regulate priming phosphorylation of specific sites and how this then leads to Rad53 activation remain poorly understood. Here we used quantitative mass spectrometry to delineate the stepwise phosphorylation events in the activation of endogenous Rad53 in response to S phase alkylation DNA damage, and we show that the two Rad9 and Mrc1 adaptors, the four N-terminal Mec1-target TQ sites of Rad53 (Rad53-SCD1), and Rad53-FHA2 coordinate intimately for optimal priming phosphorylation to support substantial Rad53 auto-activation. Rad9 or Mrc1 alone can mediate surprisingly similar Mec1 target site phosphorylation patterns of Rad53, including previously undetected tri- and tetraphosphorylation of Rad53-SCD1. Reducing the number of TQ motifs turns the SCD1 into a proportionally poorer Mec1 target, which then requires the presence of both Mrc1 and Rad9 for sufficient priming and auto-activation. The phosphothreonine-interacting Rad53-FHA domains, particularly FHA2, regulate phospho-priming by interacting with the checkpoint mediators but do not seem to play a major role in the phospho-SCD1-dependent auto-activation step. Finally, mutation of all four SCD1 TQ motifs greatly reduces Rad53 activation but does not eliminate it, and residual Rad53 activity in this mutant is dependent on Rad9 but not Mrc1. Altogether, our results provide a paradigm for how phosphorylation site clusters and checkpoint mediators can be involved in the regulation of signaling relay in protein kinase cascades *in vivo* and elucidate an SCD1-independent Rad53 auto-activation mechanism through the Rad9 pathway. The work also demonstrates the power of mass spectrometry for in-depth analyses of molecular mechanisms in cellular signaling *in vivo*.   *Molecular & Cellular Proteomics 13: 10.1074/mcp.M113.034058, 551–565, 2014.*

Eukaryotic cells are most vulnerable to exogenous DNA-damaging agents during the S phase of the cell cycle, when unprogrammed DNA lesions interfere with the tightly choreographed DNA replication process. DNA damage during this phase leads to the activation of two overlapping checkpoint pathways in *Saccharomyces cerevisiae*, the DNA replication checkpoint and the intra-S-phase DNA damage checkpoint (1, 2). Phospho-priming for auto-activation of the central checkpoint kinase Rad53 by the upstream kinase Mec1/Tel1 depends on Mrc1 as an adaptor in the DNA replication checkpoint pathway and Rad9 as an adaptor in the DNA damage checkpoint pathway (3–10). Rad53, a well-accepted model system for studying the function and regulation of Chk2-like kinases, contains two forkhead-associated (FHA)[1] domains (FHA1 and -2) and two SQ/TQ cluster domains (SCD1 and -2) enriched in Mec1/Tel1-target phosphorylation sites (11–13).

Mrc1 normally is a replisome component that functionally couples DNA Pol ε with Cdc45 and MCM helicase during replication fork progression (14, 15). As the replication forks are stalled by replication stress, the recruited checkpoint sensor kinase Mec1 phosphorylates the SCD of Mrc1, which

abolishes its N-terminal interaction with Pol ε and enables Mrc1 to recruit Rad53 and promote Rad53 phosphorylation by Mec1 as an initial step in the activation of Rad53 in the Mrc1 branch (6, 14, 16). Alanine substitution of all Mec1 target sites of Mrc1 (designated the *mrc1-AQ* allele) has been shown to selectively disable its checkpoint function for Rad53 activation without affecting its DNA replication functions (4). In response to DNA damage, Rad9 is able to associate with damaged chromatin via its BRCT and Tudor domains, which tether it to Ser129-phosphorylated histone H2A (γH2A) and Lys79-methylated histone H3, respectively (17, 18). Alternatively, the recruitment of Rad9 onto damaged DNA could also be facilitated by its phosphorylation by CDK1, which enables the specific interaction of Rad9 with Dpb11, allowing the formation of the ternary complex of Dpb11, Mec1, and Rad9 (19, 20). Similar to Mrc1, Mec1 activates the adaptor function of Rad9 by phosphorylation of its SCD, which then binds to the Rad53-FHA domains to promote Rad53 phosphorylation by Mec1 (3, 5, 10).

Beyond serving as scaffolds to recruit Rad53, Mrc1 and Rad9 have been shown to promote Rad53 phosphorylation by Mec1 in a dose-dependent manner *in vitro* (3, 16), underlining their adaptor role to enhance the enzyme–substrate (Mec1–Rad53) interaction. However, how they can specifically regulate the priming phosphorylation at specific sites and how this then leads to Rad53 activation remains poorly understood. Finally, hyperphosphorylated Rad9 has also been shown to catalyze the auto-phosphorylation of recombinant Rad53 (21), but it remains to be examined whether and how this occurs *in vivo*.

The activation of SCD-FHA containing kinases such as human Chk2 and fission yeast Cds1 has been suggested to involve a two-step phosphorylation process: first, SCD phosphorylation by an ATM/ATR-like kinase leads to intermolecular binding to the FHA domain of another Chk2/Cds1 monomer, which then results in dimerization/oligomerization-dependent auto-phosphorylation within the kinase activation loop (22–26). In addition to the characteristic N-terminal SCD-FHA module of Chk2-like kinases, Rad53 contains another SCD2-FHA2 module C-terminal to its kinase domain. Similar to its orthologues, Rad53 activation has been proposed to depend on SCD1 phosphorylation (but not SCD2 phosphorylation) and partially redundant functions of the two FHA domains (9, 27–29). However, although Rad53-FHA1 can interact with SCD1 in a phospho-threonine (pT)-dependent manner *in vitro* (9, 28), it appears to be required for Rad53 activation only in G2/M-arrested cells (27, 29). In contrast, the FHA2 domain, which seems to be more important overall for Rad53 activation, does not appreciably bind phospho-SCD1 peptides *in vitro* (27, 28). Thus, the mechanisms by which Mrc1, Rad9, SCD1 phosphorylation, and FHA domains interact during checkpoint-dependent Rad53 priming and auto-activation remain to be elucidated.

Quantitative mass spectrometric analysis has revolutionized the functional analysis of cellular signaling pathways, including site-specific phosphorylation events of key signaling molecules (30–33), but an important caveat is that MS studies often involve protein tags or nonphysiological expression levels that can interfere with normal protein functions. For example, the integration of a triple HA tag into the endogenous *RAD53* gene locus has been shown to reduce Rad53 protein levels, resulting in significantly altered checkpoint activity (34). In this study we used quantitative MS analyses to dissect the stepwise phosphorylation events of endogenous, untagged Rad53 in response to MMS-induced alkylation DNA damage and replication stress during the S phase. Together with functional analyses, our results delineate how the two Mec1 adaptors Rad9 and Mrc1 can coordinate with the four SCD1 priming sites (T5, T8, T12, and T15) to regulate the phospho-priming of Rad53 by Mec1. In addition, an SCD1-priming independent Rad53 auto-activation mechanism and the specific roles of the FHA domains during Rad53 hyperphosphorylation are also elucidated in this work.

EXPERIMENTAL PROCEDURES

Yeast Strains—All yeast strains were in the W303–1A background (with corrected *RAD5*) and contained *sml1::HIS3*. Point mutations were generated in the endogenous *RAD53* locus without residual markers or protein tags, and double mutant strains were generated via mating and tetrad dissection of spores as described in supplemental Table S1. In order to specifically detect S phase DNA damage activation of Rad53 without indirect effects from dNTP fluctuations during normal S phase (35), all experiments in this study were performed in *sml1Δ* strains.

Cell Synchronization, MMS Treatment, and Preparation of Spiked-in SILAC Standard—Yeast cells were grown in yeast peptone dextrose at 30 °C. Log phase cultures (optical density at 600 nm ≈ 0.4) were arrest in G1 phase by two pulses of α-factor treatment (9 μg/ml) for 75 min each. Cells were then washed extensively and resuspended in prewarmed yeast peptone dextrose with or without 0.05% MMS. The lysates were prepared from cells released from α-factor arrest into yeast peptone dextrose (45 min for collecting S phase Rad53) or yeast peptone dextrose containing 0.05% MMS (45 min for collecting maximal activated Rad53 in S phase). The SILAC isogenic strain (*CAN1* (plasma membrane Arg permease), *arg4::KAN lys2::NAT*) was grown in minimal dropout media supplemented with L-lysine-$^{13}C_6$,$^{15}N_2$ and L-arginine-$^{13}C_6$,$^{15}N_4$ (ISOTEC, Sigma, St. Louis, Missouri), and lysates were prepared from mid-log phase cells (OD 600 nm ~ 0.8 to 1) after 0.05% MMS treatment for 2 h.

Western Blotting and Immunoprecipitation—For Western blots, lysates were prepared using bead beating at 4 °C in lysis buffer (50 mM Tris-HCl, pH 7.5, 0.5% Nonidet P-40, 0.5% Triton-X 100, 150 mM NaCl, 5 mM EDTA, 1 mM phenylmethylsulfonyl fluoride, EDTA-free Protease Inhibitor Mixture (Roche), 5 mM sodium pyrophosphate, 50 mM sodium fluoride, 10 mM β-glycerophosphate, and Phosphatase Inhibitor Mixture (Sigma)) and separated by 8% standard SDS-PAGE. The rabbit polyclonal anti-Rad53 antibody was raised and affinity-purified using recombinant Rad53-FHA2 domain and then used for monitoring Rad53 characteristic gel shifts. Mouse monoclonal antibody EL7E1 was used for Rad53 immunoprecipitation and detection. Anti-Rad9 was raised and affinity-purified using recombinant Rad9-BRCT domain, anti-γH2A from Abcam, Cambridge, Massachusetts (ab15083), and anti-Clb5 from Santa Cruz Biotechnology, Dallas, Texas (sc6704). For Rad53 immunoprecipitation from large culture for MS analysis, ~150 to 200 mg of the lysate protein was collected as described above and adjusted to a protein concentration of about 10

mg/ml. The endogenous Rad53 was then immunoprecipitated using EL7E1 and protein-G Mag Sepharose Xtra beads from GE Healthcare (28–9670-70) at 4 °C overnight. After extensive washing of the beads with the lysis buffer and PBS with 0.1% Tween-20, the bound Rad53 and associated proteins were eluted with the SDS sample buffer. After spiking in "heavy" EL7E1 immunopurified Rad53 metabolically labeled with L-lysine-$^{13}C_6$,$^{15}N_2$ and L-arginine-$^{13}C_6$,$^{15}N_4$ (ISOTEC), the mixture was separated by 9.5% standard SDS-PAGE followed by in-gel trypsin digestion for LC-MS/MS analysis.

Enrichment of Phosphopeptides with TiO$_2$ Beads—The resulting tryptic fragments of Rad53 and co-purified proteins were incubated with 2 mg of TiO$_2$ beads (GL Science, Torrance, CA) or 50 μl of TiO$_2$ Mag Sepharose (GE Healthcare) in 1 M glycolic acid (Sigma) prepared in 80% acetonitrile with 5% (v/v) trifluoroacetic acid in water. After incubation for 30 min with vigorous shaking, the beads were washed with the above binding buffer and then with a solution of 80% acetonitrile with 1% (v/v) trifluoroacetic acid twice. The bound phosphopeptides were then eluted from the beads with 5% NH$_3$ twice. After acidification with formic acid, the eluted phosphopeptides were desalted by C$_{18}$ StageTips (Proxeon Biosystems, Thermo, Waltham, Massachusetts, USA).

LC-MS/MS and Data Analysis—The resulting peptides were generated from in-gel trypsin digestion, which cleaves at the C terminus of lysine and arginine residues. The peptide nanoflow LC-MS/MS experiments were performed using a reverse-phase C$_{18}$ capillary column and an LTQ-Orbitrap hybrid mass spectrometer (Thermo) equipped with a nanoelectrospray ion source (New Objective, Woburn, Massachusetts) and an ultrahigh pressure LC (Waters Corporation, Milford, Massachusetts, USA) or HPLC pump (Agilent Technology, Santa Clara, CA). The scan cycle was initiated with a full-scan survey MS (*m/z* 320–1600) experiment in the Orbitrap followed by data-dependent MS/MS experiments in the linear ion trap on the 12 or 20 most abundant ions detected in the full MS scan. The raw MS and MS/MS spectra were processed by MaxQuant (1.2.2.5 or 1.3.0.5) with the Andromeda search engine for protein and peptide identification in a target-decoy *Saccharomyces cerevisiae* protein database (yeast orf trans all 05-Jan-2010.fasta; 6754 entries) (36). The precursor and fragment mass tolerance were set to 6 ppm and 0.5 Da, respectively, with up to two missed cleavages. Cysteine carbamidomethylation was used as a fixed modification, and the variable modifications were methionine oxidation; protein N-terminal acetylation; asparagine deamidation; and serine, threonine, and tyrosine phosphorylation. The false discovery rate was set at 1% for peptides, proteins, and sites, and the minimum peptide length allowed was seven amino acids. In order to precisely quantitate the changes in the Rad53 phosphorylation and in the association of Mrc1 and Rad9 with Rad53, the abundance of the unlabeled and SILAC-labeled tryptic fragments was also manually examined and calculated based on the peak areas in the extracted ion chromatogram for their top three isotopic peptide precursor ions with 25 ppm mass tolerance using Xcalibur (Thermo). The results for the quantitation of Rad53 phosphorylation were obtained from two to six independent biological repeats for all of the yeast strains used in this study. The lists of all detected Rad53 tryptic fragments and Rad53 and Mrc1 phosphorylation site identifications are organized in supplemental Tables S2–S4. All annotated, mass-labeled spectra for supplemental Tables S2–S4 can be found in supplemental Table S5.

RESULTS

Quantitative MS Analysis of Endogenous Rad53 Phosphorylation in Response to S Phase DNA Damage—Whereas the Rad9-dependent DNA damage checkpoint pathway functions during all cell cycle phases, the Mrc1 pathway is only active during S phase (2, 37). Thus, in order to be able to assess the contributions of both adaptors to Rad53 activation under comparable conditions, we chose to monitor Rad53 phosphorylation in response to S phase MMS treatment. To investigate Rad53 phosphorylation under entirely physiological conditions, we took advantage of the recently developed monoclonal antibody EL7E1 (38), which can efficiently immunoprecipitate endogenous Rad53 with or without MMS (supplemental Fig. S1A). We employed a variant of the SILAC-based quantitative MS approach, "spike-in SILAC" (39), to evaluate the effects of different mutations on the site-specific phosphorylation states of Rad53 under ideal growth conditions. As shown in Fig. 1A, phosphorylation-dependent electrophoretic mobility shifts of Rad53 were maximal after the G1-arrested yeast cells had been released for 45 min into S phase in the presence of 0.05% MMS. To avoid measuring secondary responses, a 45-min MMS treatment was chosen as the standard condition in this study. As indicated in Fig. 1B, all unlabeled EL7E1 affinity-purified "light Rad53" experimental samples were internally standardized by spiking with the same amount of "heavy Rad53" reference sample prepared via DNA damage treatment of an isogenic WT strain (except for *lys2Δ arg4Δ CAN1* to ensure even labeling) grown in $^{13}C/^{15}N$-Lys/Arg containing minimal medium. The mixture of the heavy (H) and light (L) Rad53 samples was then separated by SDS-PAGE (supplemental Fig. S1B), followed by in-gel tryptic digestion and LC-MS/MS analysis using an LTQ-Orbitrap hybrid MS analyzer. The resulting peptide identification covered around 90% of the Rad53 protein sequence (supplemental Table S2). Two types of phosphopeptide analysis were performed: the relative levels of phosphorylation (the WT data were set to be 100%) using the normalized heavy phosphopeptide as the reference, and the estimated phosphostoichiometry (*i.e.* percent site occupancy) based on depletion of the corresponding unphosphorylated peptide counterpart. The detailed algorithms are further elaborated below.

As illustrated in row I of Fig. 1B, the L/H ratios of Rad53 tryptic fragments that did not contain phosphorylation or other post-translational modification sites were used to normalize the input levels of unlabeled Rad53. It was then possible to compare the relative phosphorylation levels of specific sites (or multisites) between different Rad53 samples (row II in Fig. 1B), including the *mrc1-AQ rad9Δ* control strain in which both mediator pathways are disabled, to allow identification of the checkpoint-dependent phosphorylation events. Examples of the raw precursor MS scan are shown in Fig. 1C for an unmodified Rad53$^{670-679}$ fragment as the input control (a) and the unphosphorylated (b) and mono-, di-, tri-, and tetra-phosphorylated (c–f, respectively) Rad53-SCD1 fragments (Rad53$^{1-17}$, MENI*T*QP*T*QQS*T*QA*T*QR) in unlabeled light (L1–L3) experimental samples relative to the SILAC-labeled heavy (H) DNA-damaged WT reference sample. Comparison of the
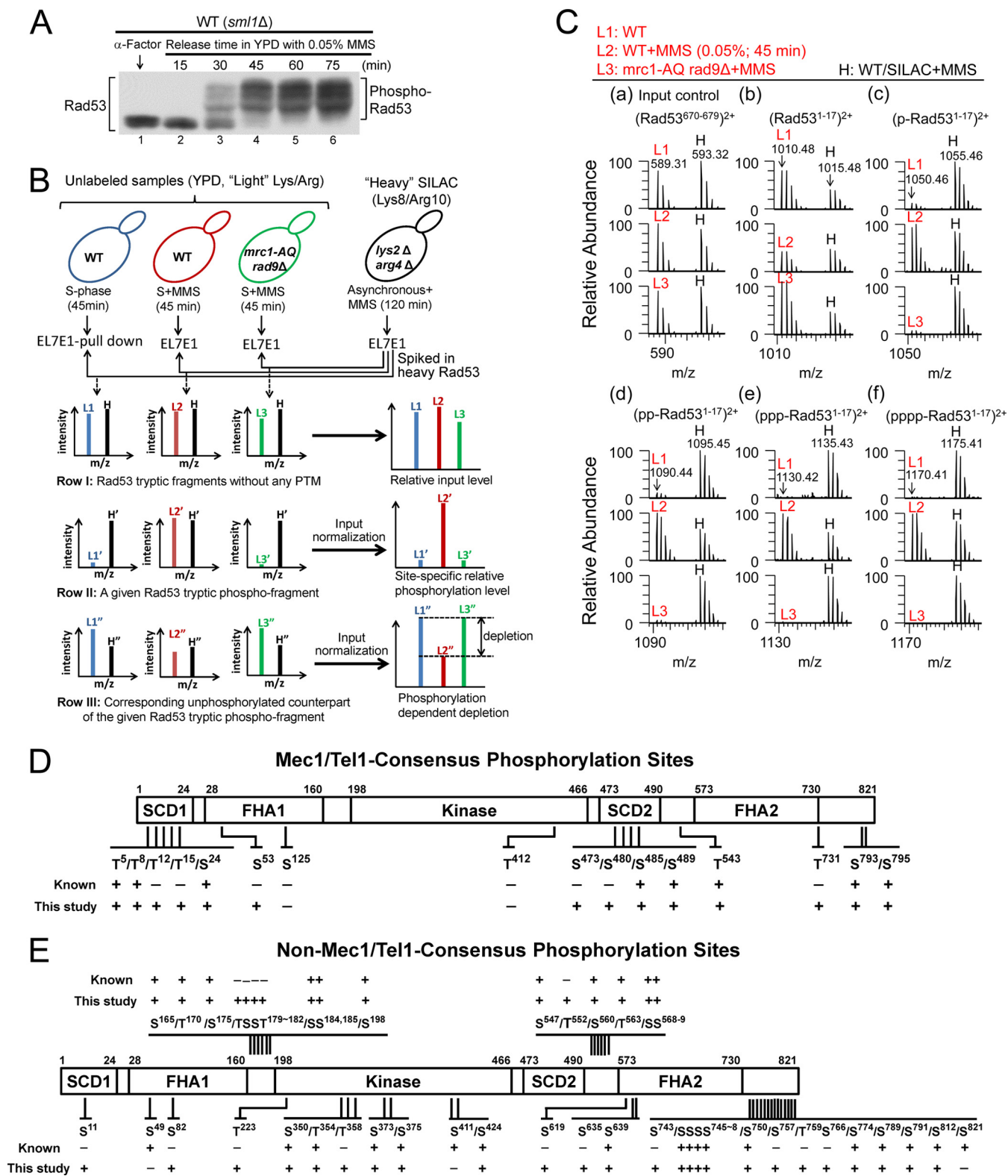
FIG. 1. **Rad53 phosphorylation site mapping in EL7E1-immuno-purified endogenous, untagged Rad53 after S phase MMS treatment.** *A*, Western blot analysis for phosphorylation-dependent electrophoretic mobility shifts of Rad53. Samples were collected during α-factor G1 arrest (0 min) and at the indicated time points after release into the S phase with 0.05% MMS. *B*, conditions and workflow of the spike-in SILAC approach to quantitate the site-specific phosphorylation level and the estimated phosphostoichiometry of Rad53. *C*, precursor mass spectral scans for an unmodified Rad53$^{670-679}$ fragment FLLQDGDEIK (a) and the unphosphorylated (b) and mono-, di-, tri-, and tetraphosphorylated

MMS-treated WT sample (L2) with the untreated sample (L1) and the *mrc1-AQ rad9Δ* control (L3) indicated that phosphorylation of the four TQ motifs (c–f) was checkpoint- and DNA-damage-dependent.

Furthermore, as phosphorylation at a given site results in lower levels of the corresponding unphosphorylated peptides (row III of Fig. 1*B*), quantitation of the relative depletion of unphosphorylated peptides compared with that in the unperturbed S phase sample allowed us to estimate the changes of phosphostoichiometry in response to DNA damage, with the caveat that in tryptic peptides with multiple phosphorylation sites (*e.g.* SCD1 or SCD2), this depletion analysis can only estimate the total fraction of phosphorylated peptides without resolution of individual sites or specific multiphosphorylation states. For example, note that as a consequence of substantial SCD1 phosphorylation after S phase checkpoint activation (Fig. 1*C*, L2, c–f), the level of the corresponding unphosphorylated SCD1 fragment Rad53[1–17] (L2, b) was considerably reduced relative to the unperturbed WT (L1, b) or the MMS-treated *mrc1-AQ rad9Δ* (L3, b).

New Phosphorylation Sites, Multisites, and Estimated Stoichiometry—Altogether, for endogenous, untagged Rad53 in response to S phase MMS treatment, we detected significantly elevated *in vivo* phosphorylation at 14 potential Mec1/Tel1-target motifs (SQ/TQs) (Figs. 1*D* and 2*A*; supplemental Fig. S2*A*; supplemental Table S3), including 6 new sites (T12, T15, S53, S473, S480, and T731) not identified in previous reports (3, 28, 40–42). We also detected phosphorylation at 41 mostly DNA damage–inducible non-SQ/TQ sites (Figs. 1*E* and 2*B*; supplemental Fig. S2*B*; supplemental Table S3), including 15 newly identified *in vivo* phosphorylation sites. Interestingly, all four TQs in SCD1 and all four SQs in SCD2 were found to be phosphorylatable and simultaneously phosphorylatable (Fig. 1*C*; supplemental Fig. S2*C*; supplemental Table S2). The MS[2] spectral assignments for identification of the tetraphosphorylated SCD1 and SCD2 peptides are shown in supplemental Figs. S2*D* and S2*E*, respectively.

It is also important to note that the phosphostoichiometry varied substantially between different sites for the DNA-damage-induced Rad53 hyperphosphorylation (Fig. 2*C*, supplemental Fig. S2*F*). The closely spaced Mec1/Tel1 phosphorylation site clusters SCD1 (T5/T8/T12/T15/S24) and SCD2 (S473/S480/S485/S489) generally showed high phosphorylation stoichiometry (>50%) in response to S phase DNA damage, and the estimated phosphostoichiometry of the critical activation loop residue T354 was about 50% (Fig. 2*C*). Taken together, the large number of phosphorylation sites and multisites and the high phosphostoichiometry of many of these sites provide a molecular explanation for the extensive electrophoretic mobility shifts of Rad53 that have been well established previously as shown in Fig. 1*A*.

Identification of Kinase-dependent Rad53 Phosphorylation Events with the Kinase-deficient rad53-K227A Allele—To functionally characterize these Rad53 phosphorylation events, we performed MS analyses in MMS-treated, otherwise isogenic strain containing the kinase-deficient *rad53-K227A* allele (43) (this section) or checkpoint mediator-deficient *mrc1-AQ*, *rad9Δ*, and double mutant *mrc1-AQ rad9Δ* strains (next section) for comparison with WT.

As shown by the relative levels of MMS-inducible phosphorylation sites (Figs. 2*A* and 2*B*; supplemental Figs. S2*A* and S2*B*) and the relative depletion of the corresponding unphosphorylated peptides (Fig. 2*C*; supplemental Fig. S2*F*), defective Rad53 kinase activity caused little or no decrease in its SQ/TQ phosphorylation states. In contrast, the relative phosphorylation levels of several non-SQ/TQ sites, including that of the key activation loop residue T354 (38, 44), were greatly diminished in the kinase-defective strain (Fig. 2*B*), indicating that these are auto-phosphorylation sites. However, some of these autokinase sites (S185, S547, S560, T563, and S635) retained minor phosphorylation levels in the kinase-defective strain, indicative of low-level transphosphorylation by other kinases (Fig. 2*B*). Another group of phosphorylation sites (supplemental Fig. S2*B*; S198, S373, S750, S766, and S789) were partially reduced in the absence of Rad53 kinase activity but still occurred relatively efficiently, suggesting that they are transphosphorylated by other kinases whose activity is directly or indirectly modulated by Rad53 activity (*e.g.* Polo kinases involved in down-regulating checkpoint activity) (40, 45, 46).

Mrc1 and Rad9 Function Redundantly in Rad53 Phosphorylation Events—In the *mrc1-AQ rad9Δ* strain, in which both mediator pathways were disabled, all of these DNA-damage-inducible phosphorylation levels were dramatically reduced (Fig. 2; supplemental Figs. S2*A*–S2*C* and S2*F*), except for residually detectable low phosphorylation levels in the SCD2 domain (Figs. 2*A*b and 2*C*a) and the C-terminal SQSQ motif (S793/S795; supplemental Figs. S2*A* and S2*F*a). Whereas disabling both mediators was detrimental to Rad53 hyperphosphorylation and activation, the single mutants *mrc1-AQ* and *rad9Δ* had surprisingly negligible effects on the phosphorylation levels at most SQ/TQ sites and the Rad53 autophosphorylation sites including the autoactivation site T354, as shown in the same set of figures. Thus, in response to alkylating DNA damage during DNA replication, the Mrc1 and Rad9 pathways appear to function virtually redundantly without any notable preference for directing Mec1 phosphorylation to particular Rad53 residues.

(c–f, respectively) SCD1 Rad53[1–17] fragment MENI*TQPTQQSTQATQ*R (the N-terminal Met was N-acetylated and S-oxidized) in unlabeled light (L1–L3) experimental samples relative to the SILAC-labeled heavy (H) DNA-damaged WT reference sample. Mass-to-charge ratio (*m/z*) of the monoisotopic precursor is labeled at each top panel. Mec1/Tel1 consensus (SQ/TQ) phosphorylation sites (*D*) and other sites (*E*) identified in this study are also presented.
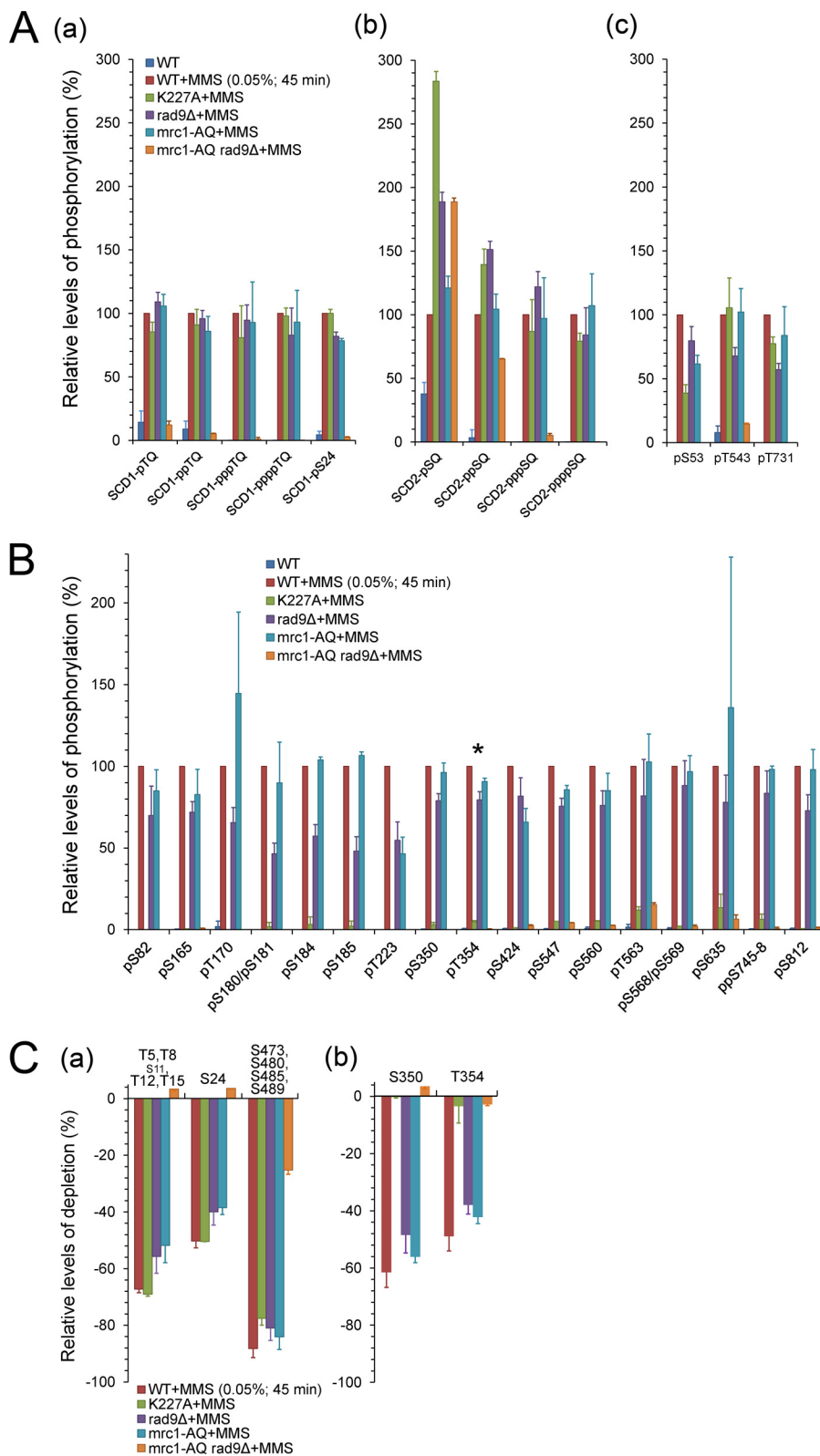
FIG. 2. **Quantitative mass spectrometric analyses of Rad53 phosphorylation upon S phase DNA damage.** *A* and *B*, bar graphs showing the relative phosphorylation levels of the DNA-damage-inducible Mec1/Tel1-target (*A*) and autophosphorylation (*B*) sites in the indicated strains after S phase MMS treatment. The asterisk (*) marks the crucial autoactivating residue T354. *C*, bar graphs showing the estimated phospho-stoichiometries of selected Mec1/Tel1-target sites (a) and autophosphorylation sites (a) based on the relative depletion ratios of the corresponding unphosphorylated peptides. Note that "S11" presented in a small font is not a Mec1/Tel1 target site.

Because the lack of identifiable pathway-specific phospho-fingerprints was surprising, we tested whether the absence of one mediator pathway leads to an increased association of Rad53 with the other adaptor for S phase DNA damage signaling. Tryptic Mrc1 phosphopeptides, mostly derived from its SCD domain, were readily detectable (supplemental Table S4)
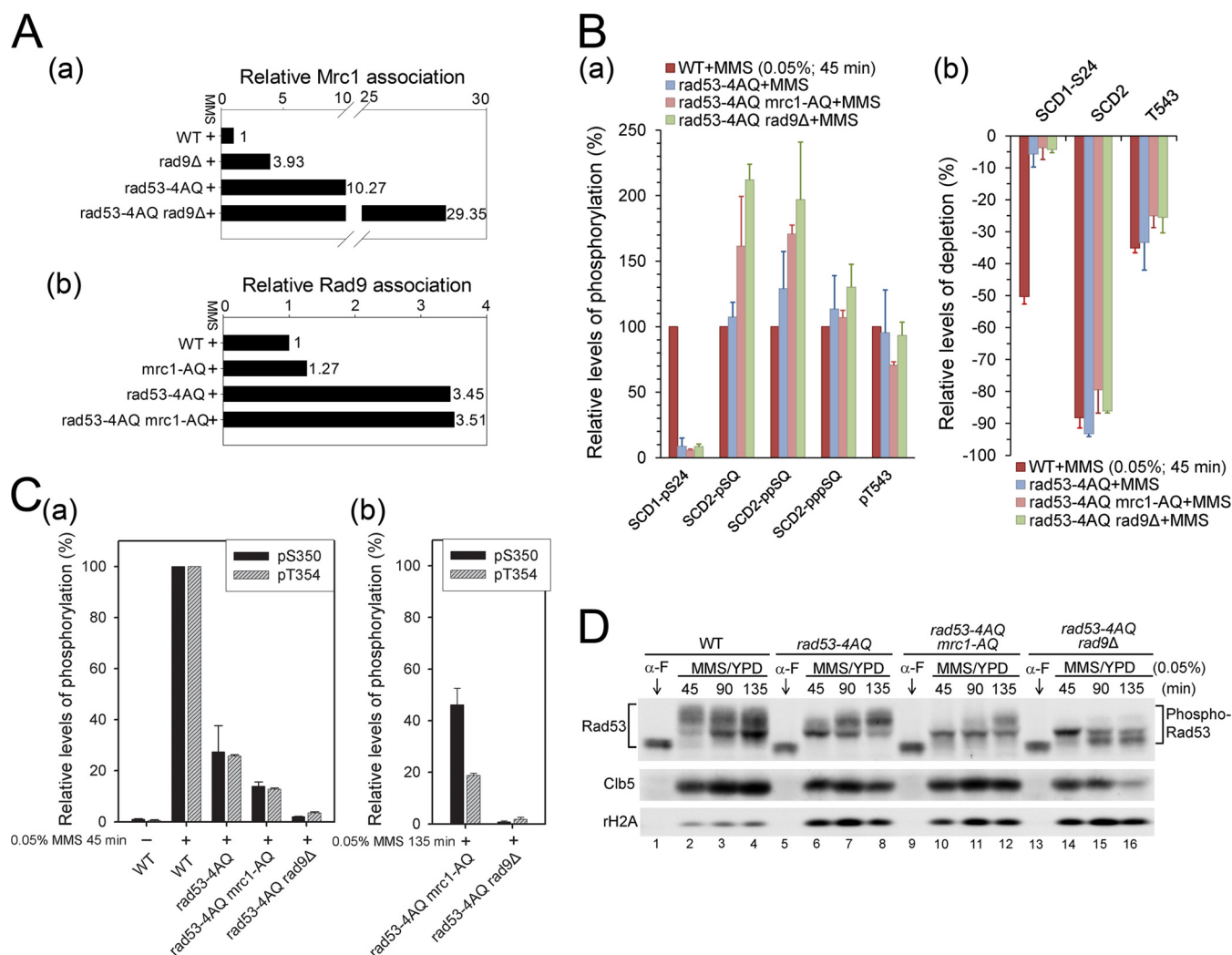
FIG. 3. **Effects of *rad9Δ*, *mrc1-AQ*, and *rad53-4AQ* on Rad53 hyperphosphorylation.** *A*, relative association levels of Mrc1 (a) and Rad9 (b) with Rad53 during MMS-perturbed S phase in the indicated strains. See supplemental Figs. S3A and S3B for raw MS spectra used for quantitation. *B*, effects of SCD1, Rad9, and Mrc1 mutations on the relative phosphorylation levels (a) and the phosphostoichiometries based on depletion ratios of corresponding unphosphorylated peptides (b) for selected high-stoichiometric SQ/TQ phosphorylation sites. *C*, effects of SCD1, Rad9, and Mrc1 mutations on the relative phosphorylation levels of S350 and T354 within the activation loop after 45 min (a) and 135 min (b) of MMS treatment in S phase. See supplemental Fig. S3C for additional MS quantitation of Rad53 autophosphorylation. *D*, Western blot analysis for phosphorylation-dependent electrophoretic mobility shifts of Rad53. Clb5 and γH2A are shown as S phase and DNA damage markers, respectively. Samples were collected during α-factor G1 arrest (0 min) and at the indicated time points after release into the S phase with 0.05% MMS.

and quantifiable (supplemental Fig. S3A) in Rad53 immune complexes by MS analysis after TiO₂ enrichment (47). Relative to levels in the MMS-treated WT, the level of Rad53-associated Mrc1 increased by ~3-fold in the *rad9Δ* strain (Fig. 3*A*a; supplemental Fig. S3A). Conversely, the level of Rad9 association in similar analyses of the *mrc1-AQ* strain increased by only ~30% relative to the MMS-treated WT (Fig. 3*A*b; supplemental Fig. S3B). Thus, compensation for the absence of Rad9 may involve relative hyperactivation of the Mrc1 branch, whereas the Rad9 branch may already be highly engaged and competent to deal with S phase DNA damage without the need for significant hyperactivation in the absence of the Mrc1 checkpoint branch.

SCD1 Phospho-priming Is a Key Regulator but Not Sole Determinant of Rad53 Autoactivation—The integrity of the SCD1 TQ cluster has previously been reported to be required for efficient Rad53 activation (9, 28), and our MS results showed that all four TQs were indeed phosphorylatable during S phase DNA damage responses (Fig. 1*C*; supplemental Fig. S2D). To directly assess the importance of SCD1 for Rad53 trans- and autophosphorylation, we analyzed phospho-patterns in the *rad53-4AQ* strain, in which these four threonine residues are replaced by alanine. The 4AQ mutation had little effect on the phosphorylation of other SQ/TQ motifs, except S24 in the same SQ/TQ cluster (Fig. 3*B*). In contrast, it led to a profound reduction in the phosphorylation of all

autophosphorylation sites (supplemental Fig. S3Ca), including the key autoactivation site pT354 as well as pS350 in the kinase activation loop, which were reduced to 25.8% ± 0.5% and 27% ± 10% of WT levels, respectively (Fig. 3Ca). This was also supported by Western blot analysis of phosphorylation-dependent electrophoretic Rad53 mobility shifts in response to S phase MMS treatment, which were considerably reduced in *rad53-4AQ* at 45 min, when the WT showed maximal shifts (Fig. 3D, lanes 2 and 6). In addition, the activation of Rad53^{4AQ} was considerably slower than that of the WT (lanes 1–2 and 5–8), and this strain accumulated higher γH2A levels (Fig. 3D, lower panel, lanes 5–8), suggesting increased replicative DNA damage (48). Together, these results confirm the importance of SCD1 phosphorylation for efficient Rad53 activation, but they also indicate that autoactivation can be accomplished via an alternative, though less efficient, mechanism without phospho-primed SCD1.

Rad9 but Not Mrc1 Also Functions as a Scaffold for SCD1-independent Rad53 Autoactivation—The finding that Rad53 was unaffected by single *mrc1-AQ* or *rad9Δ* mutations prompted us to test whether either of these pathways was involved in the residual Rad53 autoactivation in the *rad53-4AQ* strain. Interestingly, the combined absence of SCD1 phosphorylation sites and Rad9 in *rad53-4AQ rad9Δ* almost completely abolished the activating Rad53 autophosphorylation at T354, whereas this effect was considerably more modest in the *rad53-4AQ mrc1-AQ* double mutant (Fig. 3C; supplemental Fig. S3C). In line with the results of autophosphorylation, MMS-induced Rad53 mobility shifts were further reduced relative to *rad53-4AQ* in both double mutants at 45 min (Fig. 3D, lanes 6, 10, and 14), but the autophosphorylation and the mobility shifts increased at later time points in *rad53-4AQ mrc1-AQ* but not *rad53-4AQ rad9Δ* (Fig. 3D, lanes 9–16; supplemental Fig. S3Cb). These results suggest that Rad9 is essential for residual Rad53 activation in the absence of SCD1 phosphorylation, whereas the Mrc1 branch plays only a relatively minor role in the SCD1-independent pathway. As neither *mrc1-AQ* nor *rad9Δ* had substantial effects on the phosphorylation of other Rad53 SQ/TQ sites in *rad53-4AQ* (Fig. 3B), Rad9 cannot fulfill this SCD1-independent function by increasing phosphorylation of other SQ/TQ sites during the priming step. Collectively, these results suggest that, in addition to mediating phospho-priming, Rad9 is able to directly contribute to the activating autophosphorylation step as a scaffold catalyst at physiological protein levels *in vivo*, as proposed based on biochemical reconstitution assays *in vitro* (21).

We next analyzed the relative associations of Mrc1 and Rad9 with immunoprecipitated Rad53 under these conditions. Based on MS (Fig. 3Ab; supplemental Fig. S3B) and immunoprecipitation/Western blot analyses (supplemental Fig. S3D), Rad9 association with Rad53 after 45 min of S phase MMS treatment increased by ~2.5-fold in *rad53-4AQ* as well as in *rad53-4AQ mrc1-AQ* strains relative to that in the

WT strain. In contrast, under the same conditions, Mrc1 association with Rad53 increased by ~10-fold relative to the WT in *rad53-4AQ*, and by almost 30-fold in *rad53-4AQ rad9Δ* (Fig. 3Aa; supplemental Fig. S3A). The finding that despite highly increased Mrc1 association Rad53 cannot be activated in *rad53-4AQ rad9Δ* cells demonstrates that Mrc1 cannot substitute for Rad9 in the residual SCD1-independent autoactivation mechanism. Together, these results indicate that Rad9 can contribute to both steps of Rad53 activation *in vivo*, whereas Mrc1 regulates only the priming step in response to S phase MMS damage.

Both Mrc1 and Rad9 Adaptors Are Required for Sufficient SCD1 Priming Phosphorylation when Fewer SCD1-TQ Motifs Are Preserved—It has been suggested previously that a single threonine in Rad53-SCD1, with preference for T8, is largely sufficient to prime Rad53 for activation (28). This was confirmed here, as *rad53-T8-3AQ* maintained 70% ± 10% of WT T354 autophosphorylation, compared with 25.8% ± 0.5% in *rad53-4AQ* (Fig. 4A; supplemental Fig. S4Aa). However, this was no longer true in the absence of Rad9, where the corresponding figures were 13.7% ± 0.3% in *rad53-T8-3AQ rad9Δ* and 3.5% ± 0.4% in *rad53-4AQ rad9Δ* (Fig. 4A; supplemental Fig. S4Ab). We thus quantified the phosphorylation state of SCD1 in these strains. Interestingly, the relative level of T8 phosphorylation in *rad53-T8-3AQ* was reduced to ~40% when *RAD9* was deleted (Fig. 4B; supplemental Fig. S4B). This result is in contrast to the WT, in which the deletion of *RAD9* did not significantly affect the level of SCD1 phosphorylation (Fig. 2Aa). These results suggest that reducing the number of TQ motifs could render SCD1 a poorer Mec1 target in the absence of Rad9, leading to impaired phospho-priming.

We then examined the effect of *mrc1Δ* on the levels of pT8 and activation loop phosphorylation in *rad53-T8-3AQ*. As indicated in Fig. 4B and supplemental Fig. S4C, the induction of pT8 in *rad53-T8-3AQ* was also reduced to ~36% when *MRC1* was deleted. In accordance with the impaired phospho-priming, the corresponding pT354 was reduced to 25% ± 3% of WT levels in *rad53-T8-3AQ mrc1Δ* (Fig. 4C). Taken together, the results suggest that the presence of both mediators is required for sufficient phosphorylation of T8 in the absence of other N-terminal TQ motifs in *rad53-T8-3AQ*.

We next examined whether increasing the number of SCD1 TQ motifs improved Rad53 activation in the absence of Rad9 or Mrc1 by increasing the overall likelihood of SCD1 phosphorylation. In *rad53-T5T8-2AQ rad9Δ* or *rad53-T5T8-2AQ mrc1Δ*, although the relative levels of mono- and diphosphorylated SCD1 fragments were still lower than those in *rad53-T5T8-2AQ* with WT *RAD9* and *MRC1* (Fig. 4D; supplemental Fig. S4D), the availability of two TQs not only led to certain levels of diphosphorylated species (Fig. 4Db) but also alleviated the reduction of the relative levels of SCD1 monophosphorylation (Fig. 4Da) compared with the effect of *rad9Δ* or *mrc1Δ* on the *rad53-T8-3AQ* mutant in Fig. 4B. Furthermore, when all four SCD1 TQs were available, we observed minimal
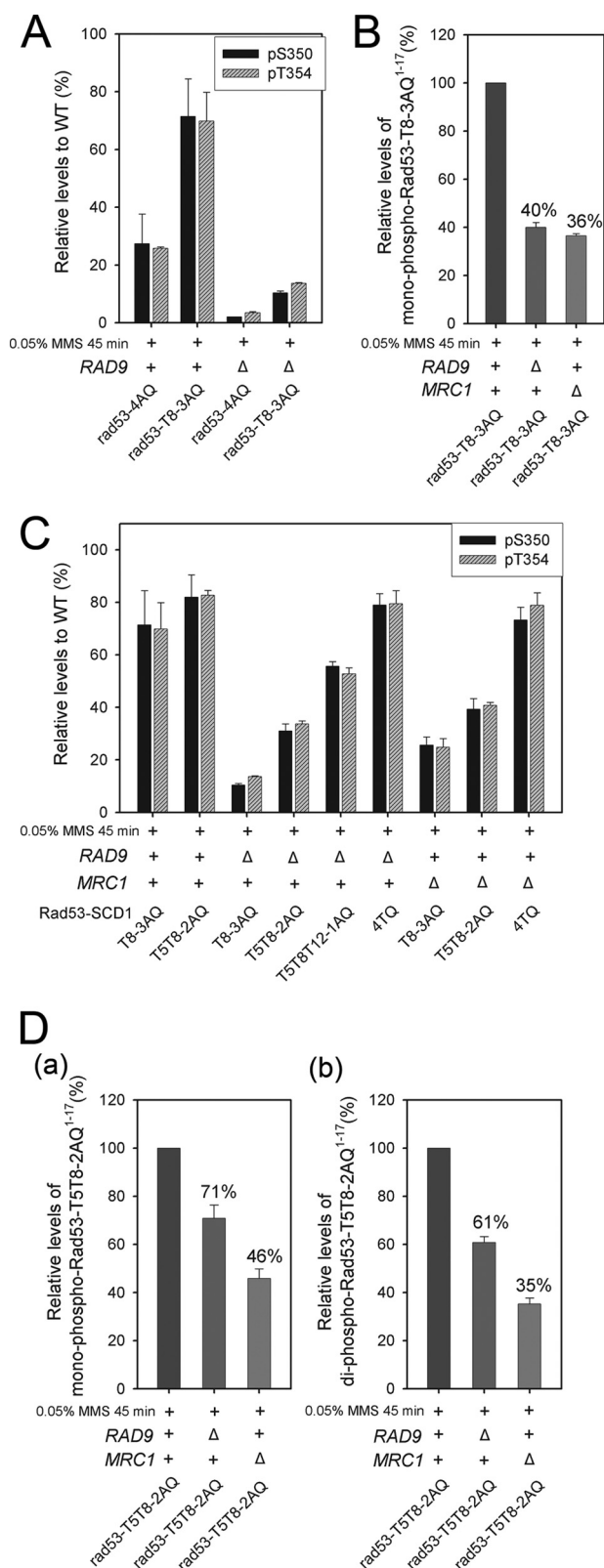
FIG. 4. **Multiple SCD1 TQ motifs are required for efficient Rad53 priming and autoactivation when either Mec1 adaptor is abolished.** *A*, *C*, relative S350 and T354 phosphorylation levels in the indicated strains. *B*, effect of *rad9Δ* or *mrc1Δ* on the relative levels of monophos-

effects on SCD1 phosphorylation in *rad9Δ* and *mrc1-AQ* (Figs. 2*A* and 2*C*) or *mrc1Δ* (supplemental Fig. S4*E*). These results suggest that the presence of multiple TQs enables the efficient phosphorylation of SCD1 in the presence of a single Mec1 adaptor. In light of the effects in promoting the overall levels of priming SCD1 phosphorylation, the preservation of more TQs in SCD1 proportionally improved the autoactivating T354 phosphorylation when either Rad9 or Mrc1 was absent (Fig. 4*C*; supplemental Figs. S4*A*b and S4*A*c). Similar results were obtained for pS350 within the activation loop (Fig. 4*C*), as well as for most of the other high-occupancy autophosphorylation sites (data not shown). This correlation between the level of priming phosphorylation and the phosphorylation at the activation loop demonstrates that the autoactivation of Rad53 is highly regulated by the priming efficiency. Altogether, whereas an intact TQ cluster supports efficient priming phosphorylation of SCD1 when only one of the Mec1 adaptors is present, reducing the number of TQ motifs turns SCD1 into a proportionally poorer Mec1 target, which then requires both Mrc1 and Rad9 for sufficient priming phosphorylation to support substantial Rad53 autoactivation.

Multiple SCD1 Threonines Are Required for RAD53-dependent DNA Damage Survival in the Absence of the Mrc1 or Rad9 Adaptor—Because Rad53 activity plays a key role in DNA damage survival, we performed DNA damage survival assays to assess the biological significance of these findings. Similar to T354 phosphorylation, relative to results in *rad53-4AQ*, preserving a single SCD1 threonine in *rad53-T8-3AQ* (or *rad53-T5-3AQ*) improved MMS survival to near the WT level in the presence of both mediators (Fig. 5*A*). In accordance with the effects on pT354, when combined with *rad9Δ*, a single threonine in SCD1 (*rad53-T5-3AQ rad9Δ* or *rad53-T8-3AQ rad9Δ*) only modestly improved the extreme MMS hypersensitivity relative to *rad53-4AQ rad9Δ*, with further gradual survival improvements with the preservation of two (*rad53-T5T8-2AQ rad9Δ*) or three threonines (*rad53-T5T8T12-1AQ rad9Δ* or *rad53-T5T8T15-1AQ rad9Δ*) (Fig. 5*A*). Similar results were also observed for the effect of *mrc1Δ* on fewer TQ preserved SCD1 mutants, though with less attenuation than in the effect by *rad9Δ* (Fig. 5*B*). This is likely because Mrc1 carries out the adaptor function in response to replication stress mainly during S phase (6), whereas Rad9 is required throughout the cell cycle in response to DNA damage (2, 4, 37). Like in the regulation for Rad53 autoactivation, multiple SCD1 priming sites are required for sustaining *Rad53*-dependent DNA damage survival in the presence of a single Mec1 adaptor.

phorylated rad53-T8-3AQ[1–17] fragment MENI*AQP*TQQS*AQ*AAQR in Rad53[T8-3AQ]. See supplemental Figs. S4*B and S4*C for the raw extracted ion chromatogram data used for quantitation. *D*, effect of *rad9Δ* or *mrc1Δ* on the relative levels of mono- (a) and diphosphorylated (b) rad53-T5T8-2AQ[1–17] fragment MENI*TQP*TQQS*AQ*AAQR in Rad53[T5T8-2AQ]. See supplemental Fig. S4*D* for the raw extracted ion chromatogram data used for quantitation.
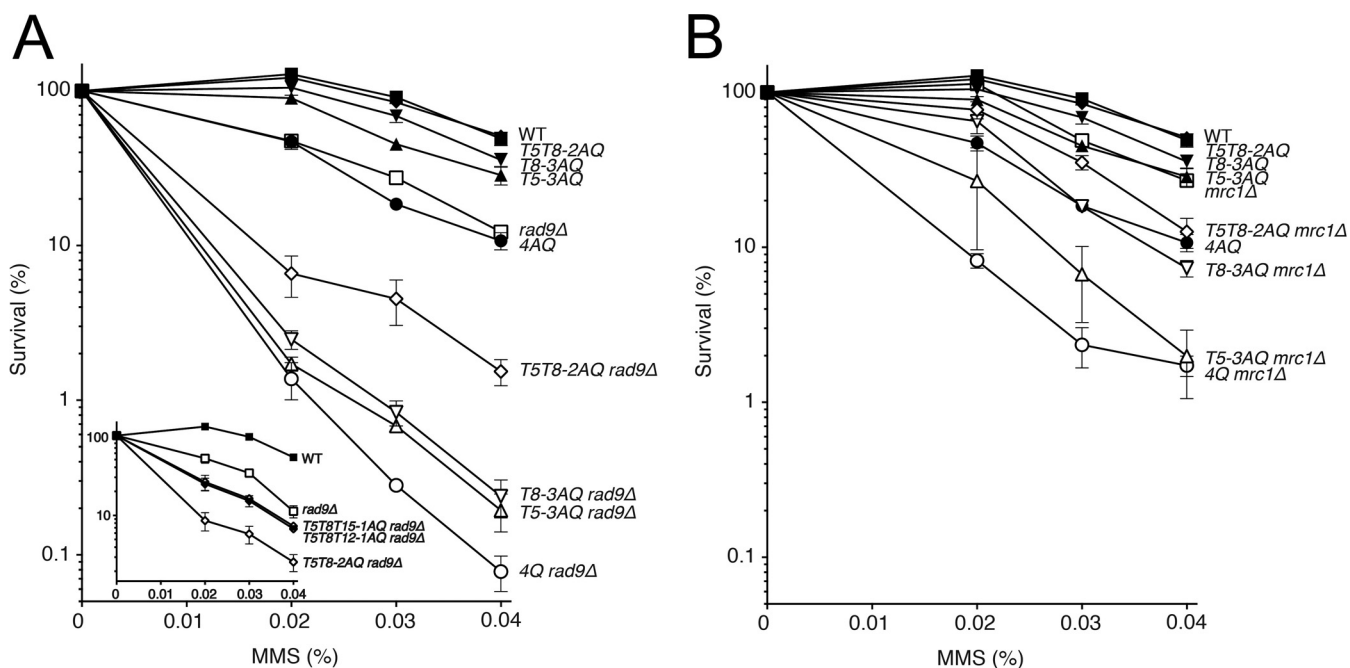
FIG. 5. **Multiple SCD1 TQ motifs are required for sustaining *RAD53*-dependent DNA damage survival in the presence of a single Mec1 adaptor.** Clonal survival assays of the indicated SCD1 mutants in the presence and absence of Rad9 (*A*) or Mrc1 (*B*). Unsynchronized cultures were treated with the indicated doses of MMS for 3 h and plated on yeast peptone dextrose medium. Survival was calculated from the fraction of colonies formed relative to the untreated control.

The FHA2 Domain Plays a Major Role in SCD1 Priming Phosphorylation—The FHA-mediated binding of Rad53 to Rad9 and Mrc1 has been shown to be involved in its phospho-priming by Mec1 (3, 5, 8, 10, 16). We therefore examined the contribution of Rad53-FHA domains to the phosphorylation of Rad53. We analyzed the phospho-pattern in *rad53-R70A*, *rad53-R605A*, and *rad53-R70A-R605A* strains upon S phase DNA damage, when the pT binding ability of FHA1 and/or FHA2 is specifically impaired by alanine substitution of the respective critical arginine residue (27, 29, 49–51). As indicated by the Western blot analysis of Rad53 mobility shifts (Fig. 6*A*), hyperphosphorylation of Rad53 depends mainly on the pT binding activity of FHA2, and FHA1 is required only for residual Rad53 phosphorylation in the absence of a functional FHA2 domain.

We then used MS-based relative depletion analysis to evaluate the effects of FHA mutations on the total phosphorylation within the SCD1 priming site cluster. As shown in Figs. 6*B* and 6*C*, the phosphorylation-dependent depletion of unphosphorylated Rad53$^{1-17}$ (MENI*TQP TQQS TQAT Q*R) was significantly reduced in *rad53-R605A*, but not in *rad53-R70A,* suggesting that the priming phosphorylation of Rad53 by Mec1 is predominantly mediated by FHA2. Similar to the results of Rad53 mobility shifts (Fig. 6*A*), SCD1 priming was further reduced in *rad53-R70A-R605A* (Figs. 6*B* and 6*C*), indicative of a low level of redundancy between the two FHA domains in Rad53 priming. In accordance with the decreased levels of SCD1 priming phosphorylation in *rad53-R605A* and *rad53-R70A-R605A*, the

relative phosphorylation levels of the autoactivating T354, as well as other high-stoichiometric autophosphorylation sites, also decreased correspondingly (Fig. 6*D*a). Together, these results suggest that the phospho-priming of Rad53 is predominantly contributed by the pT binding activity of FHA2, which is crucial for sustaining the hyperphosphorylation of Rad53 upon S phase DNA damage.

FHA1-pSCD1 Binding Is Not the Major Regulator for Rad53 Autoactivation—Relative to Rad53-FHA2, Rad53-FHA1 has been linked to a much wider range of interaction partners (9, 10, 28, 52–56), in particular the phosphorylated Rad53-SCD1 since the intermolecular interaction of phospho-SCD/FHA is widely believed to be a paradigm for the autoactivation mechanism of Chk2-like kinases (22–26). However, the finding that *rad53-R70A* did not significantly impair Rad53 autophosphorylation (Fig. 6*D*a), while on the other hand *rad53-4AQ* showed substantial impairment of Rad53 autophosphorylation (Fig. 3*C*; supplemental Fig. S3*C*), raised the possibility that FHA1-pSCD1 binding might not play a major role in the autoactivation of Rad53. To test this possibility, we studied the pattern of Rad53 autophosphorylation in the absence of Rad9 (*rad53-4AQ rad9Δ* and *rad53-R70A rad9Δ*) that allows for selective assessment of the SCD1-specific autoactivation pathway. As indicated in Fig. 6*D*b, whereas the SCD1 mutation almost completely abolished the total levels of pT354 and other autophosphorylation sites in *rad9Δ*, the FHA1 mutation caused only a modest effect when combined with *rad9Δ*. These results suggest that, in contrast to other Chk2-like
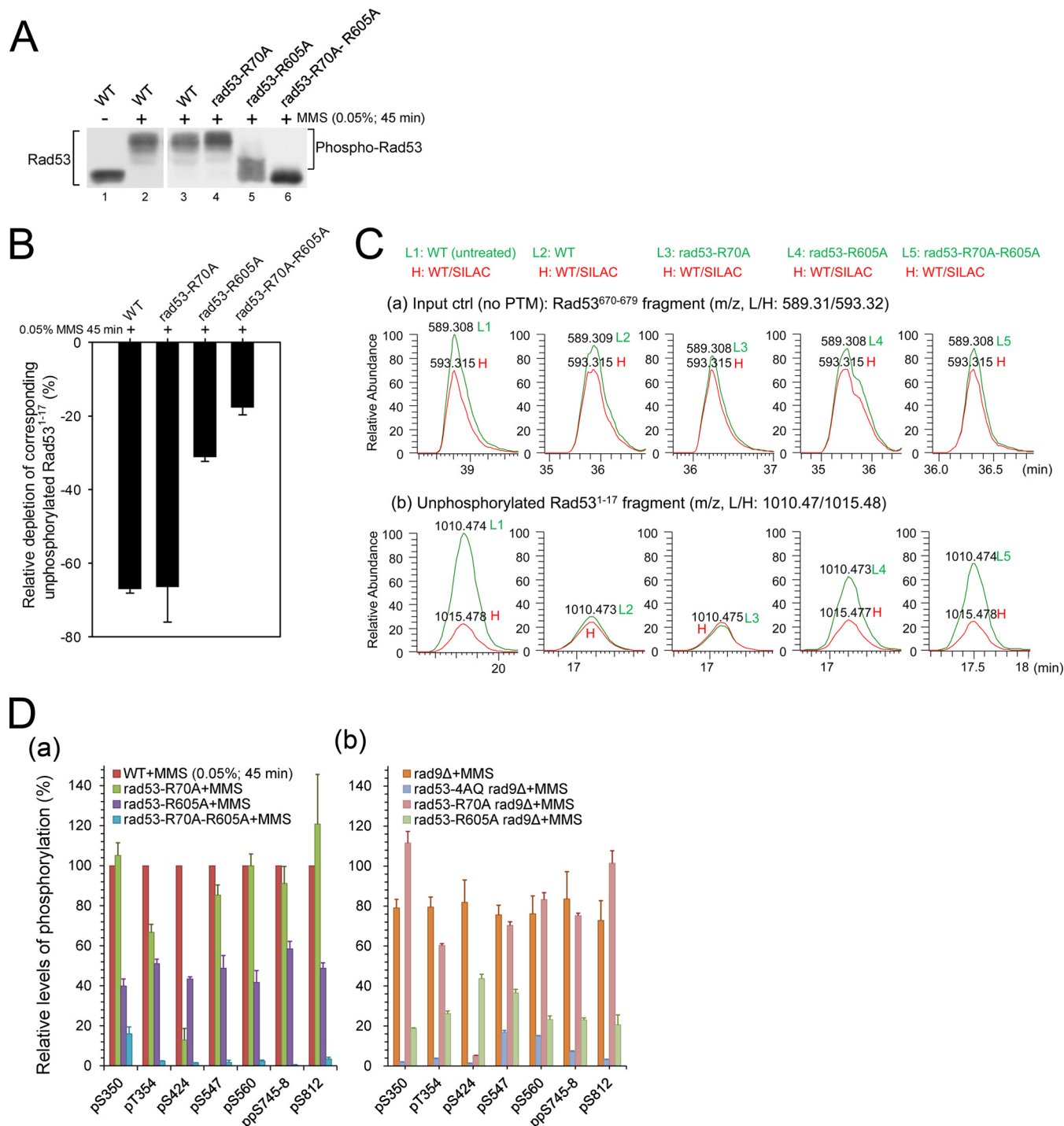
FIG. 6. **FHA domain functions in the regulation of Rad53 hyperphosphorylation.** *A*, Western blot analysis for phosphorylation-dependent electrophoretic mobility shifts of Rad53 in the indicated strains. Samples were collected after 45 min of 0.05% MMS treatment in S phase. *B*, effects of the indicated FHA mutations on the depletion ratios of the corresponding unphosphorylated Rad53$^{1-17}$ fragment. *C*, monoisotopic peak extracted ion chromatograms (with 25 ppm tolerance) for an unmodified Rad53$^{670-679}$ fragment (a) and the unphosphorylated Rad53$^{1-17}$ fragment (b) in the indicated, unlabeled light strains relative to the normalized spiked-in heavy DNA-damaged WT references. Note that L1 and L2 peaks in (a) and (b) here correspond to those in Figs. 1*C*a and 1*C*b, except that only the monoisotopic peak is outputted here in an expanded view. *D*, effects of the indicated FHA, SCD1, and Rad9 mutations on the relative phosphorylation levels of selected high-stoichiometric autophosphorylation sites.

FIG. 7. **Proposed models for the priming and autoactivation mechanisms of Rad53 upon S phase alkylation DNA damage.** *A*, proposed models for the formation of Rad53 priming complexes in Mrc1-mediated DNA replication checkpoint and Rad9-mediated DNA damage checkpoint pathways. Mrc1 and Rad9 phosphorylation by Mec1 (step 1) enable the recruitment of Rad53 for priming by Mec1 via binding to Rad53-FHA2 (step 2). The re-priming of Rad53 may occur to ensure a sufficient level of priming phosphorylation (step 3), which promotes substantial Rad53 autoactivation. *B*, proposed models of possible intermediate complexes I and II involved in the *in vivo* autoactivation of Rad53.
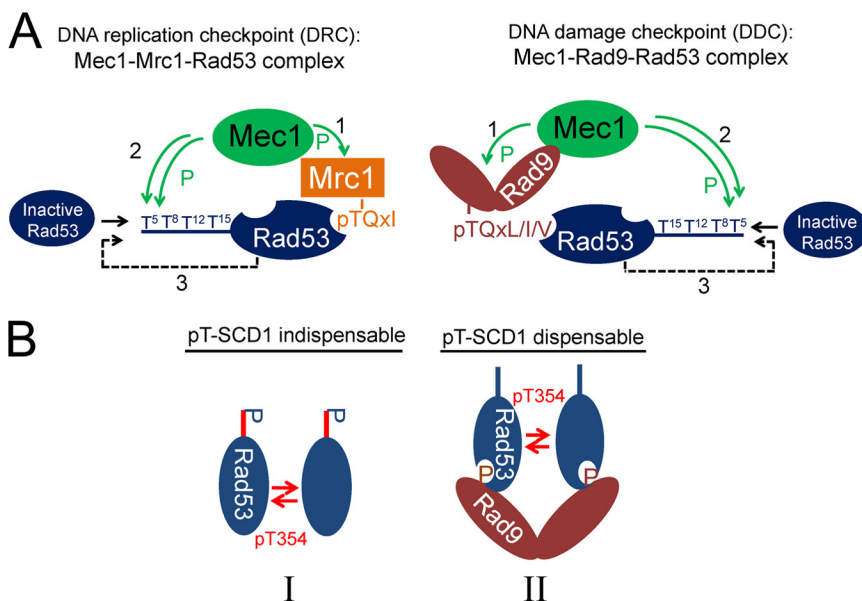
kinases, FHA1-pSCD1 interactions cannot be the major mechanism in the pSCD1-specific Rad53 autoactivation step in response to S phase alkylation DNA damage.

Relative to *rad53-R70A rad9Δ*, *rad53-R605A rad9Δ* led to a more pronounced defect in Rad53 autophosphorylation (Fig. 6*D*b). This result, however, does not suggest a major role of FHA2 in the pSCD1-specific Rad53 autoactivation either, because it can be attributed to the noticeably impaired phospho-priming in the SCD1 domain in *rad53-R605A rad9Δ* (but not in *rad53-R70A rad9Δ*) (supplemental Fig. S5). The results in supplemental Fig. S5 also suggest that in the absence of Rad9, FHA2 still plays a major role in the priming of SCD1, presumably via the Mrc1 pathway.

DISCUSSION

In this study, we combined advanced mass spectrometric quantification of phosphorylation site occupancy and mutational analyses to delineate the specific roles of Rad9, Mrc1, and Rad53 SCD1 and FHA1/2 domains in the activation of endogenous Rad53 in response to S phase DNA damage treatment *in vivo*. The studies led to four major findings regarding the phospho-priming step: (i) As a Mec1 adaptor, Mrc1 and Rad9 can function redundantly (one is sufficient) when all four TQs are present. (ii) Reciprocally, the TQ motifs can function redundantly (one is sufficient) when both adaptors are present. (iii) However, the priming is impaired when neither the two adaptors nor the four TQ sites are intact. Under these circumstances, the priming efficiency is proportional to the number of TQ motifs. (iv) FHA2 plays a major role in the interaction of Rad53 with Rad9 or Mrc1 for Rad53 priming by Mec1. These features are incorporated into a model shown in Fig. 7*A*.

The studies also identified three significant mechanistic features for the autoactivation step: (i) The level of autophos-

phorylation is correlated with the priming efficiency (*i.e.* the overall phosphorylation stoichiometry of the TQ cluster). (ii) However, in contrast to the other Chk2-like kinases, the priming-mediated Rad53 activation does not seem to involve direct binding between the FHA1 domain and phosphorylated SCD1 as the major mechanism, though a minor role cannot be ruled out. (iii) In the absence of TQ sites, Rad9 but not Mrc1 can mediate an SCD1-independent activation mechanism of Rad53, though with less efficiency.

Possible Molecular Basis for the Redundant Functions of Mrc1 and Rad9 in the Phospho-priming Step—Although our finding that Rad9 and Mrc1 function redundantly during the Rad53 priming step is consistent with previous observations (6), it should be stressed that there was not a single transphosphorylation site "sentinel" specific for the Mrc1- or Rad9-associated checkpoint pathway during MMS-damaged S phase (Fig. 2*A*; supplemental Fig. S2*A*), which suggests that both scaffolds recruit Rad53 in a structurally very similar manner for priming by Mec1, as illustrated by the model shown in Fig. 7*A*. Interaction of Mec1-phosphorylated pTQxL/I/V in Rad9 with the Rad53-FHA2 domain has previously been proposed to be important for Rad53 priming by Mec1 (5). Interestingly, our MS analysis of Rad53-interacting protein tryptic fragments revealed several different Mrc1 peptides containing phosphorylated pTQxI motifs (supplemental Table S4), which fits with the preferential phospho-ligand specificity of Rad53-FHA2 (49). Based on this, together with our finding that the pT-binding activity of FHA2 is critical for Rad53 priming (Figs. 6*A*–6*C*), it seems reasonable to speculate that the interaction of Rad53-FHA2 with Mrc1-pTQxI or Rad9-pTQxL/I/V could likely be the major structural basis for the redundant functions of Mrc1 and Rad9 in the phospho-priming step of Rad53 activation. In contrast to the ability of Rad9 to dimerize or oligomerize *in vivo* (20, 21, 57), Mrc1 monomers

are believed to be stably tethered to Polε and the replisome with only its Mec1-phosphorylated N-terminal region available for Rad53 binding (14), which could explain its inability to dimerize Rad53 for the autoactivation step.

Coordination of Mec1 Adaptors and Mec1 Target Sites for Optimal Priming of Rad53 by Mec1—Although the redundancy of four individual priming sites in Rad53 activation has been suggested previously based on the study of single TQ-preserved SCD1 (9, 28), here we found that both mediators, Mrc1 and Rad9, are required for sufficient phospho-priming through a single priming site in order to facilitate efficient Rad53 autoactivation (Fig. 4). Likewise, although the potential redundant roles of Mrc1 and Rad9 in S phase Rad53 activation have been reported previously (6), we found that they were no longer redundant when the number of TQ sites was limited. Taken together, our results demonstrate for the first time the coordination between the multiple adaptors and the multiple TQ sites—when the adaptor is only minimally available, the priming sites need to be maximally available, and vice versa.

Possible Intermediate Complexes of Rad53 Autoactivation—The detailed phosphorylation results obtained with various mutants allow us to propose two alternative Rad53 autoactivation intermediates for the *in vivo* autoactivation of Rad53 (Fig. 7*B*). In intermediate I, the inactive Rad53 could possibly be dimerized for activation-loop phosphorylation in a pT-SCD1-dependent manner. Note that in addition to mono-pT-SCD1-Rad53, we also observed di-, tri-, and tetra-pT-SCD1-Rad53 (Figs. 1*C* and 2*A*a; supplemental Table S2). It remains to be established, however, whether multiphosphorylated SCD1 is also involved or even favored in this mechanism. In II, the inactive Rad53 with or without SCD1 phosphorylation can be dimerized via Rad9 scaffolds, mainly by tethering to the Mec1-phosphorylated Rad9-SCD involving its FHA domains (3, 5, 8, 10). Because SCD1 is highly phosphorylated in the WT upon MMS-induced DNA damage during S phase (Fig. 2*C*), and because ablation of the four SCD1 TQ motifs in *rad53-4AQ* has a much greater effect than deletion of Rad9 on the autoactivation of Rad53 (Figs. 2*B* and 3*C*), we believe that the pT-SCD1-indispensable intermediate I is the favorable route in sustaining Rad53 autoactivation.

Given that direct FHA1-pT-SCD1 binding does not seem to be a major mechanism in Rad53 autoactivation and that FHA2 (which is key to the priming step) does not bind pSCD1 with appreciable affinity (9, 28), we propose the possible involvement of an unknown scaffold protein in intermediate I, which either could be able to dimerize or may contain at least two separate pT-binding regions to facilitate dimerization of SCD1-phospho-primed Rad53. Potential candidates that fulfill this requirement include the dimeric 14-3-3 proteins Bmh1 and Bmh2, which have previously been shown to bind Rad53 and affect its activation (58, 59), and the multi-BRCT domain containing proteins Esc4/Rtt107 and Dbp11, which are associated with damage sites and have also been linked to multi-

ple roles in checkpoint regulation (19, 60–62). These candidates, however, were not detected in our preliminary proteomic analyses of binding partners in *rad53-4AQ* and the WT (only Dun1 was shown to be stably associated with WT Rad53 but not rad53[4AQ]), which nonetheless does not rule out their involvement in Rad53 activation, as formation of the activation complex could be very transient.

Implication for the in Vivo Activation Mechanisms of Rad53 and Other Chk2-like Kinases—Here we have combined the power of yeast genetics to introduce specific point mutations without the need for residual selection markers that may indirectly affect protein levels and functions (63), a Rad53-specific monoclonal antibody to efficiently purify the endogenous untagged protein, and advanced mass spectrometry to study Rad53 activation under physiological conditions. This approach has enabled the detection of numerous novel Rad53 *in vivo* phosphorylation sites for which the kinases responsible may have been limiting under substrate overexpression conditions, and the results suggest that the crucial autoactivation step of Chk2-like kinases does not always need to involve direct phospho-SCD1/FHA domain interactions. Although the important finding we have uncovered for Rad53 might be unique for those fungal Chk2-like kinases that contain duplicate SCD-FHA modules, the notion that physiological analyses are crucial for the study of Rad53 activation might prompt similar analyses to revisit the role of individual phosphorylation sites in the *in vivo* regulation of mammalian Chk2-like kinases. Regardless of whether the mechanisms deciphered here are applicable to mammalian checkpoint responses, all proteins studied here—Rad53, Mrc1, and Rad9—are highly conserved in human pathogenic fungi such as *Candida*, where they are involved in regulating the switch to more invasive and drug-resistant hyphal growth forms (64, 65), and where they might represent potential drug targets to stop the spread of nosocomial fungal infections.

REFERENCES

1. Nyberg, K. A., Michelson, R. J., Putnam, C. W., and Weinert, T. A. (2002) Toward maintaining the genome: DNA damage and replication checkpoints. *Annu. Rev. Genet.* **36,** 617–656
2. Melo, J., and Toczyski, D. (2002) A unified view of the DNA-damage checkpoint. *Curr. Opin. Cell Biol.* **14,** 237–245

3. Sweeney, F. D., Yang, F., Chi, A., Shabanowitz, J., Hunt, D. F., and Durocher, D. (2005) *Saccharomyces cerevisiae* Rad9 acts as a Mec1 adaptor to allow Rad53 activation. *Curr. Biol.* **15,** 1364–1375

4. Osborn, A. J., and Elledge, S. J. (2003) Mrc1 is a replication fork component whose phosphorylation in response to DNA replication stress activates Rad53. *Genes Dev.* **17,** 1755–1767

5. Schwartz, M. F., Duong, J. K., Sun, Z., Morrow, J. S., Pradhan, D., and Stern, D. F. (2002) Rad9 phosphorylation sites couple Rad53 to the *Saccharomyces cerevisiae* DNA damage checkpoint. *Mol. Cell* **9,** 1055–1065

6. Alcasabas, A. A., Osborn, A. J., Bachant, J., Hu, F., Werler, P. J., Bousset, K., Furuya, K., Diffley, J. F., Carr, A. M., and Elledge, S. J. (2001) Mrc1 transduces signals of DNA replication stress to activate Rad53. *Nat. Cell Biol.* **3,** 958–965

7. Ma, J.-L., Lee, S.-J., Duong, J. K., and Stern, D. F. (2006) Activation of the checkpoint kinase Rad53 by the phosphatidyl inositol linase-like kinase Mec1. *J. Biol. Chem.* **281,** 3954–3963

8. Schwartz, M. F., Lee, S. J., Duong, J. K., Eminaga, S., and Stern, D. F. (2003) FHA domain-mediated DNA checkpoint regulation of Rad53. *Cell Cycle* **2,** 384–396

9. Lee, S.-J., Schwartz, M. F., Duong, J. K., and Stern, D. F. (2003) Rad53 phosphorylation site clusters are important for Rad53 regulation and signaling. *Mol. Cell Biol.* **23,** 6300–6314

10. Sun, Z., Hsiao, J., Fay, D. S., and Stern, D. F. (1998) Rad53 FHA domain associated with phosphorylated Rad9 in the DNA damage checkpoint. *Science* **281,** 272–274

11. Mahajan, A., Yuan, C., Lee, H., Chen, E. S. W., Wu, P.-Y., and Tsai, M.-D. (2008) Structure and function of the phosphothreonine-specific FHA domain. *Sci. Signal.* **1,** re12

12. Antoni, L., Sodha, N., Collins, I., and Garrett, M. D. (2007) CHK2 kinase: cancer susceptibility and cancer therapy—two sides of the same coin? *Nat. Rev. Cancer* **7,** 925–936

13. Traven, A., and Heierhorst, J. (2005) SQ/TQ cluster domains: concentrated ATM/ATR kinase phosphorylation site regions in DNA-damage-response proteins. *Bioessays* **27,** 397–407

14. Lou, H., Komata, M., Katou, Y., Guan, Z., Reis, C. C., Budd, M., Shirahige, K., and Campbell, J. L. (2008) Mrc1 and DNA polymerase [var epsilon] function together in linking DNA replication and the S phase checkpoint. *Mol. Cell* **32,** 106–117

15. Szyjka, S. J., Viggiani, C. J., and Aparicio, O. M. (2005) Mrc1 is required for normal progression of replication forks throughout chromatin in *S. cerevisiae*. *Mol. Cell* **19,** 691–697

16. Chen, S.-H., and Zhou, H. (2009) Reconstitution of Rad53 activation by Mec1 through adaptor protein Mrc1. *J. Biol. Chem.* **284,** 18593–18604

17. Hammet, A., Magill, C., Heierhorst, J., and Jackson, S. P. (2007) Rad9 BRCT domain interaction with phosphorylated H2AX regulates the G1 checkpoint in budding yeast. *EMBO Rep.* **8,** 851–857

18. Wysocki, R., Javaheri, A., Allard, S., Sha, F., Côté, J., and Kron, S. J. (2005) Role of Dot1-dependent histone H3 methylation in G1 and S phase DNA damage checkpoint functions of Rad9. *Mol. Cell. Biol.* **25,** 8430–8443

19. Pfander, B., and Diffley, J. F. X. (2011) Dpb11 coordinates Mec1 kinase activation with cell cycle-regulated Rad9 recruitment. *EMBO J.* **30,** 4897–4907

20. Granata, M., Lazzaro, F., Novarina, D., Panigada, D., Puddu, F., Abreu, C. M., Kumar, R., Grenon, M., Lowndes, N. F., Plevani, P., and Muzi-Falconi, M. (2010) Dynamics of Rad9 chromatin binding and checkpoint function are mediated by its dimerization and are cell cycle–regulated by CDK1 activity. *PLoS Genet.* **6,** e1001047

21. Gilbert, C. S., Green, C. M., and Lowndes, N. F. (2001) Budding yeast Rad9 is an ATP-dependent Rad53 activating machine. *Mol. Cell* **8,** 129–136

22. Ahn, J.-Y., Li, X., Davis, H. L., and Canman, C. E. (2002) Phosphorylation of threonine 68 promotes oligomerization and autophosphorylation of the Chk2 protein kinase via the forkhead-associated domain. *J. Biol. Chem.* **277,** 19389–19395

23. Li, J., Taylor, I. A., Lloyd, J., Clapperton, J. A., Howell, S., MacMillan, D., and Smerdon, S. J. (2008) Chk2 oligomerization studied by phospho-peptide ligation. *J. Biol. Chem.* **283,** 36019–36030

24. Oliver, A. W., Paul, A., Boxall, K. J., Barrie, S. E., Aherne, G. W., Garrett, M. D., Mittnacht, S., and Pearl, L. H. (2006) Trans-activation of the DNA-damage signalling protein kinase Chk2 by T-loop exchange. *EMBO J.* **25,** 3179–3190

25. Xu, Y.-j., Davenport, M., and Kelly, T. J. (2006) Two-stage mechanism for activation of the DNA replication checkpoint kinase Cds1 in fission yeast. *Genes Dev.* **20,** 990–1003

26. Xu, X., Tsvetkov, L. M., and Stern, D. F. (2002) Chk2 activation and phosphorylation-dependent oligomerization. *Mol. Cell. Biol.* **22,** 4419–4432

27. Pike, B. L., Yongkiettrakul, S., Tsai, M.-D., and Heierhorst, J. (2003) Diverse but overlapping functions of the two forkhead-associated (FHA) domains in Rad53 checkpoint kinase activation. *J. Biol. Chem.* **278,** 30421–30424

28. Lee, H., Yuan, C., Hammet, A., Mahajan, A., Chen, E. S., Wu, M. R., Su, M. I., Heierhorst, J., and Tsai, M. D. (2008) Diphosphothreonine-specific interaction between an SQ/TQ cluster and an FHA domain in the Rad53-Dun1 kinase cascade. *Mol. Cell* **30,** 767–778

29. Pike, B. L., Tenis, N., and Heierhorst, J. (2004) Rad53 kinase activation-independent replication checkpoint function of the N-terminal forkhead-associated (FHA1) domain. *J. Biol. Chem.* **279,** 39636–39644

30. Old, W. M., Shabb, J. B., Houel, S., Wang, H., Couts, K. L., Yen, C.-Y., Litman, E. S., Croy, C. H., Meyer-Arendt, K., Miranda, J. G., Brown, R. A., Witze, E. S., Schweppe, R. E., Resing, K. A., and Ahn, N. G. (2009) Functional proteomics identifies targets of phosphorylation by B-Raf signaling in melanoma. *Mol. Cell* **34,** 115–131

31. Guo, X., Ward, M. D., Tiedebohl, J. B., Oden, Y. M., Nyalwidhe, J. O., and Semmes, O. J. (2010) Interdependent phosphorylation within the kinase domain T-loop regulates CHK2 activity. *J. Biol. Chem.* **285,** 33348–33357

32. Scales, T., Derkinderen, P., Leung, K.-Y., Byers, H., Ward, M., Price, C., Bird, I., Perera, T., Kellie, S., Williamson, R., Anderton, B., and Reynolds, C. H. (2011) Tyrosine phosphorylation of tau by the SRC family kinases Lck and Fyn. *Mol. Neurodegener.* **6,** 12

33. Jin, L. L., Tong, J., Prakash, A., Peterman, S. M., St-Germain, J. R., Taylor, P., Trudel, S., and Moran, M. F. (2010) Measurement of protein phosphorylation stoichiometry by selected reaction monitoring mass spectrometry. *J. Proteome Res.* **9,** 2752–2761

34. Cordon-Preciado, V., Ufano, S., and Bueno, A. (2006) Limiting amounts of budding yeast Rad53 S-phase checkpoint activity results in increased resistance to DNA alkylation damage. *Nucleic Acids Res.* **34,** 5852–5862

35. Hoch, N. C., Chen, E. S.-W., Buckland, R., Wang, S.-C., Fazio, A., Hammet, A., Pellicioli, A., Chabes, A., Tsai, M.-D., and Heierhorst, J. (2013) Molecular basis of the essential S phase function of the Rad53 checkpoint kinase. *Mol. Cell. Biol.* **33,** 3202–3213

36. Cox, J., and Mann, M. (2008) MaxQuant enables high peptide identification rates, individualized p.p.b.-range mass accuracies and proteome-wide protein quantification. *Nat. Biotechnol.* **26,** 1367–1372

37. Pellicioli, A., and Foiani, M. (2005) Signal transduction: how Rad53 kinase is activated. *Curr. Biol.* **15,** R769-R771

38. Fiorani, S., Mimun, G., Caleca, L., Piccini, D., and Pellicioli, A. (2008) Characterization of the activation domain of the Rad53 checkpoint kinase. *Cell Cycle* **7,** 493–499

39. Geiger, T., Wisniewski, J. R., Cox, J., Zanivan, S., Kruger, M., Ishihama, Y., and Mann, M. (2011) Use of stable isotope labeling by amino acids in cell culture as a spike-in standard in quantitative proteomics. *Nat. Protoc.* **6,** 147–157

40. Schleker, T., Shimada, K., Sack, R., Pike, B. L., and Gasser, S. M. (2010) Cell cycle-dependent phosphorylation of Rad53 kinase by Cdc5 and Cdc28 modulates checkpoint adaptation. *Cell Cycle* **9,** 350–363

41. Smolka, M. B., Albuquerque, C. P., Chen, S.-H., Schmidt, K. H., Wei, X. X., Kolodner, R. D., and Zhou, H. (2005) Dynamic changes in protein-protein interaction and protein phosphorylation probed with amine-reactive isotope tag. *Mol. Cell. Proteomics* **4,** 1358–1369

42. Albuquerque, C. P., Smolka, M. B., Payne, S. H., Bafna, V., Eng, J., and Zhou, H. (2008) A multidimensional chromatography technology for in-depth phosphoproteome analysis. *Mol. Cell. Proteomics* **7,** 1389–1396

43. Fay, D. S., Sun, Z., and Stern, D. F. (1997) Mutations in SPK1/RAD53 that specifically abolish checkpoint but not growth-related functions. *Curr. Genet.* **31,** 97–105

44. Chen, S.-H., Smolka, M. B., and Zhou, H. (2007) Mechanism of Dun1 activation by Rad53 phosphorylation in *Saccharomyces cerevisiae*. *J. Biol. Chem.* **282,** 986–995

45. Vidanes, G. M., Sweeney, F. D., Galicia, S., Cheung, S., Doyle, J. P., Durocher, D., and Toczyski, D. P. (2010) CDC5 inhibits the hyperphosphorylation of the checkpoint kinase Rad53, leading to checkpoint adaptation. *PLoS Biol.* **8,** e1000286

46. Donnianni, R. A., Ferrari, M., Lazzaro, F., Clerici, M., Tamilselvan Nach-imuthu, B., Plevani, P., Muzi-Falconi, M., and Pellicioli, A. (2010) Elevated levels of the polo kinase Cdc5 override the Mec1/ATR checkpoint in budding yeast by acting at different steps of the signaling pathway. *PLoS Genet.* **6,** e1000763

47. Sugiyama, N., Masuda, T., Shinoda, K., Nakamura, A., Tomita, M., and Ishihama, Y. (2007) Phosphopeptide enrichment by aliphatic hydroxy acid-modified metal oxide chromatography for nano-LC-MS/MS in pro-teomics applications. *Mol. Cell. Proteomics* **6,** 1103–1109

48. Cobb, J. A., Schleker, T., Rojas, V., Bjergbaek, L., Tercero, J. A., and Gasser, S. M. (2005) Replisome instability, fork collapse, and gross chromosomal rearrangements arise synergistically from Mec1 kinase and RecQ helicase mutations. *Genes Dev.* **19,** 3055–3069

49. Durocher, D., Taylor, I. A., Sarbassova, D., Haire, L. F., Westcott, S. L., Jackson, S. P., Smerdon, S. J., and Yaffe, M. B. (2000) The molecular basis of FHA domain:phosphopeptide binding specificity and implica-tions for phospho-dependent signaling mechanisms. *Mol. Cell* **6,** 1169–1182

50. Liao, H., Yuan, C., Su, M.-I., Yongkiettrakul, S., Qin, D., Li, H., Byeon, I.-J. L., Pei, D., and Tsai, M.-D. (2000) Structure of the FHA1 domain of yeast Rad53 and identification of binding sites for both FHA1 and its target protein Rad9. *J. Mol. Biol.* **304,** 941–951

51. Liao, H., Byeon, I.-J. L., and Tsai, M.-D. (1999) Structure and function of a new phosphopeptide-binding domain containing the FHA2 of rad53. *J. Mol. Biol.* **294,** 1041–1049

52. Smolka, M. B., Chen, S.-H., Maddox, P. S., Enserink, J. M., Albuquerque, C. P., Wei, X. X., Desai, A., Kolodner, R. D., and Zhou, H. (2006) An FHA domain-mediated protein interaction network of Rad53 reveals its role in polarized cell growth. *J. Cell Biol.* **175,** 743–753

53. Aucher, W., Becker, E., Ma, E., Miron, S., Martel, A., Ochsenbein, F., Marsolier-Kergoat, M.-C., and Guerois, R. (2010) A strategy for interac-tion site prediction between phospho-binding modules and their partners identified from proteomic data. *Mol. Cell. Proteomics* **9,** 2745–2759

54. Guillemain, G., Ma, E., Mauger, S., Miron, S., Thai, R., Guerois, R., Ochsen-bein, F., and Marsolier-Kergoat, M.-C. (2007) Mechanisms of checkpoint kinase Rad53 inactivation after a double-strand break in *Saccharomyces cerevisiae*. *Mol. Cell Biol.* **27,** 3378–3389

55. Pike, B. L., Yongkiettrakul, S., Tsai, M. D., and Heierhorst, J. (2004) Mdt1, a novel Rad53 FHA1 domain-interacting protein, modulates DNA dam-age tolerance and G(2)/M cell cycle progression in *Saccharomyces cerevisiae*. *Mol. Cell Biol.* **24,** 2779–2788

56. Matthews, L. A., Jones, D. R., Prasad, A. A., Duncker, B. P., and Guarné, A. (2012) *Saccharomyces cerevisiae* Dbf4 has unique fold necessary for interaction with Rad53 kinase. *J. Biol. Chem.* **287,** 2378–2387

57. Usui, T., Foster, S. S., and Petrini, J. H. J. (2009) Maintenance of the DNA-damage checkpoint requires DNA-damage-induced mediator pro-tein oligomerization. *Mol. Cell* **33,** 147–159

58. Usui, T., and Petrini, J. H. J. (2007) The *Saccharomyces cerevisiae* 14-3-3 proteins Bmh1 and Bmh2 directly influence the DNA damage-dependent functions of Rad53. *Proc. Natl. Acad. Sci. U.S.A.* **104,** 2797–2802

59. Lottersberger, F., Rubert, F., Baldo, V., Lucchini, G., and Longhese, M. P. (2003) Functions of *Saccharomyces cerevisiae* 14-3-3 proteins in re-sponse to DNA damage and to DNA replication stress. *Genetics* **165,** 1717–1732

60. Roberts, T. M., Zaidi, I. W., Vaisica, J. A., Peter, M., and Brown, G. W. (2008) Regulation of Rtt107 recruitment to stalled DNA replication forks by the cullin Rtt101 and the Rtt109 acetyltransferase. *Mol. Biol. Cell* **19,** 171–180

61. Mordes, D. A., Nam, E. A., and Cortez, D. (2008) Dpb11 activates the Mec1–Ddc2 complex. *Proc. Natl. Acad. Sci. U.S.A.* **105,** 18730–18734

62. Rouse, J. (2004) Esc4p, a new target of Mec1p (ATR), promotes resumption of DNA synthesis after DNA damage. *EMBO J.* **23,** 1188–1197

63. Breslow, D. K., Cameron, D. M., Collins, S. R., Schuldiner, M., Stewart-Ornstein, J., Newman, H. W., Braun, S., Madhani, H. D., Krogan, N. J., and Weissman, J. S. (2008) A comprehensive strategy enabling high-resolution functional analysis of the yeast genome. *Nat. Methods* **5,** 711–718

64. Jiang, Y. W., and Kang, C. M. (2003) Induction of *S. cerevisiae* filamentous differentiation by slowed DNA synthesis involves Mec1, Rad53 and Swe1 checkpoint proteins. *Mol. Biol. Cell* **14,** 5116–5124

65. Shi, Q.-M., Wang, Y.-M., Zheng, X.-D., Teck Ho Lee, R., and Wang, Y. (2007) Critical role of DNA checkpoints in mediating genotoxic-stress-induced filamentous growth in *Candida albicans*. *Mol. Biol. Cell* **18,** 815–826